

Water–gas shift kinetics over lanthanum-promoted iron catalyst in Fischer–Tropsch synthesis: thermodynamic analysis of nanoparticle size effect

Ali Nakhaei Pour · Mohammad Reza Housaindokht · Farshad Torabi

Received: 15 August 2013 / Accepted: 12 February 2014 / Published online: 7 March 2014
© Iranian Chemical Society 2014

Abstract The kinetic parameters of water–gas shift (WGS) reaction in the Fischer–Tropsch synthesis (FTS) on lanthanum-promoted iron catalyst are analyzed by size-dependent thermodynamic method. A Langmuir–Hinshelwood kinetic equation is considered for the catalysts activity evaluation. A series of unsupported iron catalysts with different particle sizes are prepared via microemulsion method. These results show that the iron particle size has considerable effects on reactants adsorption and WGS kinetic parameters and WGS activity pass from a maximum by increasing the catalyst particle size. Finally, the analysis of data showed that by increasing the iron particle from 14 to 41 nm, the WGS activation energies and heats of adsorption of carbon monoxide and water on catalysts increased from 68 to 83, 22 to 28 and 75 to 94 kJ/mol, respectively.

Keywords Fischer–Tropsch synthesis · Water–gas shift · Iron-based catalyst · Size dependent · Kinetic parameters

Introduction

The Fischer–Tropsch synthesis (FTS) has been recognized as an important alternate technology to petroleum refining in producing liquid fuels and chemicals from syngas derived from coal, natural gas and other carbon-containing

materials [1–6]. Fe-based catalyst often selected for the FTS, over its competitor of Co-based catalyst, because of its water–gas shift (WGS) activity for working in a wide range of H₂/CO feed ratio [7–10]. In literature, it has been assumed that carbon dioxide is formed by a subsequent (independent) WGS reaction and most of the carbon dioxide is formed by a following reaction occurring on a different catalytic site than FTS [11–13]. Thus, the FTS (hydrocarbon formation) and WGS (carbon dioxide formation) reactions can be described with separate kinetic expressions.

It has been stated that FTS and WGS reactions are surface phenomenon and affected by metal available on surface of catalyst [14–16]. A rule of thumb in heterogeneous catalysis is that smaller metal crystallites provide the largest surface area on which the reaction may happen [17, 18]. Therefore, it is expected that the smaller metal particle size provides more active sites. Also, nanoparticles often have superior or even new catalytic properties following from their nanometric size that give them increased surface-to-volume ratios and adjusted chemical potentials, as compared to their bulk counterparts [19–21]. Since major advances were achieved in the past decade in understanding the structural sensitivity of transition metal on surface reaction chemistry, the kinetic analysis helps to understand how structure sensitivity affects FTS and WGS activities [21–24].

Thermodynamic method for evaluation of nanoparticle size effects on the adsorption, chemical kinetic and rates is started by Parmon [25] and developed by Murzin [26–29]. The key in thermodynamic analysis method is evaluation of the particles nanometric size effects on chemical potential of active phase (e.g., clusters supported on a carrier) [30, 31]. Murzin [27–29] reported that FTS reaction on supported cobalt-based catalyst shows high sensitivity to cobalt particle size. He developed a useful method

A. Nakhaei Pour (✉) · M. R. Housaindokht
Department of Chemistry, Ferdowsi University of Mashhad,
P. O. Box: 9177948974, Mashhad, Iran
e-mail: nakhaeipoura@yahoo.com; a.nakhaei@um.ac.ir

F. Torabi
Research Institute of Petroleum Industry (RIPI),
P. O. Box: 14665-137 Tehran, Iran

for evaluation of structure sensitivity of heterogeneous catalytic reaction. Also new results showed that nano-sized iron particles play an essential role to achieve high FTS activity [11, 32–35]. Iron-based catalysts are usually used without any support, but the major inconveniences related to employing of massive catalysts are their physical degradation and low surface area [7, 36, 37].

In our previous works, we studied the effect of nanoparticles on physico-chemical, textural properties and catalytic activity of iron catalysts in FTS reaction [21, 22, 32, 34, 38–40]. The objective of this work is to provide a theoretical basis for developing size-dependent WGS kinetic equation, which is consistent with the existing knowledge in the area of Fischer–Tropsch synthesis. The rate equation will be tested with data from iron-based catalysts in a continuously operated, essentially gradientless, autoclave reactor.

Experimental

Catalyst preparation and characterization

The Fe/Cu/La catalysts with different particle size prepared as described previously [21, 34, 38–40]. The catalyst compositions are designated by the atomic ratios as: 100Fe/5.64Cu/2La. Characterizations of catalysts are reported in previous works [32, 34, 38, 39].

Experimental apparatus and procedure

Steady-state FTS reaction rates were measured in a continuous spinning basket reactor. A detailed description of the experimental setup and procedures has been provided in our previous works [14]. The fresh catalyst crushed and sieved to particles with the diameter of 0.25–0.36 mm (40–60 ASTM mesh). The weight of the catalyst loaded was 2.5 g and diluted by 30 cm³ inert silica sand with the same mesh size range. The samples activated by a 5 % (v/v) H₂/N₂ gas mixture with space velocity equal to 15.1 nl h⁻¹ g_{Fe}⁻¹ at 1 bar and 1,800 rpm. The reactor temperature increased to 673 K with a heating rate of 5 K/min, kept for 1 h at this temperature, and then reduced to 543 K. The activation followed by the synthesis gas stream with H₂/CO ratio of 1 and space velocity equal to 3.07 nl h⁻¹ g_{Fe}⁻¹ for 24 h at 1 bar and 543 K before setting the FTS reaction temperature and pressure.

After catalyst activation, synthesis gas fed to the reactor at 563 K, 17 bar, H₂/CO ratio of 1 and a space velocity equal to 10.4 nl h⁻¹ g_{Fe}⁻¹. After reaching steady state, the kinetic of the FTS rate was measured. Experimental conditions varied in the following ranges: pressure = 13–25 bar, temperature = 543–603 K, GHSV = 2.8–14 nl h⁻¹ g_{cat}⁻¹, H₂/CO

feed ratio = 0.5–2.0. Each experiment replicated three times to verify the experimental data accuracy and reproducibility.

Conversion of carbon monoxide and hydrogen and formation of various products were measured within a time period of 24 h at each run. At regular intervals, the standard experiment repeated to control possible deactivation of the catalysts. For each condition, it took at least 12 h to ensure the steady-state behavior of the catalyst after a change in the reaction conditions.

The out gas was analyzed by a gas chromatograph (Varian CP-3800) equipped with TCD and FID detectors. The CO, CO₂, N₂, and O₂ were analyzed through two packed column in series (molecular sieve 13 × CP 81025 with 2 m length, and 3 mm OD, and Hayesep Q CP1069 with 4 m length, and 3 mm OD) connected to TCD detector. The C₁–C₅ hydrocarbons were analyzed via a capillary column (CP fused silica with 25 m × 0.25 mm × 0.2 μm film thickness) connected to FID detector. Hydrogen analyzed through Shimadzu, GC PTF 4C, equipped with TCD detector and two column in series (Propack-Q with 2 m length, and 3 mm OD for CO₂, C₂H₄ and C₂H₆ separation and molecular sieve-5A with 2 m length, and 3mm OD for CO, N₂, CH₄ and O₂ separation), which connected to each other via a three way valve.

The liquid products (Including hydrocarbons and oxygenates) analyzed offline with Varian CP-3800 gas chromatograph, which is equipped with capillary column (TM DH fused silica capillary column, PETRO COL 100 m × 0.25 mm × 0.5 μm film thickness) and FID detector. Total mass balances performed with the carbon material balance closed between 97 and 103 %. This criterion was adopted since compounds containing carbon and hydrogen might accumulate in the reactor in the form of high molecular weight hydrocarbons.

Size-dependent kinetic model

Based on size-dependent thermodynamic approach, adsorption on nanoclusters changes the Gibbs energy. This phenomenon should be account for the chemical potential changes:

$$\begin{aligned} \Delta G_{\text{ads}}(r) &= \Delta G_{\text{ads},\infty} \pm \mu_i(r) \mp \mu_{\infty} = \Delta G_{\text{ads},\infty} \pm \delta(r) \\ &= \Delta G_{\text{ads},\infty} \pm \frac{2\sigma V_M}{r} \end{aligned} \quad (1)$$

where r is dimension of average catalyst particle size, μ_{∞} is the standard chemical potential of the bulk phase, $\delta(r)$ is the chemical potential increment, V_M is the partial molar volume of the substance forming the condensed phase and σ is the surface tension. Depending on the nature of the bonding interactions of the molecule with the nanoparticle

surface as compared to that of the bulk material (here the bulk materials refer to particles with micrometer or larger diameters), the change in adsorption-free energy from the nanosize effect can be positive or negative.

If K_{ads} increases with decreasing particle size, which suggests a stronger adsorption to the nanoparticle surface as compared to that to the bulk surface. Therefore, the change in adsorption-free energy from the nanosize effect is negative, that is, $\Delta G_{ads}(r) = \Delta G_{ads,\infty} - \delta(r)$. From this negative change in adsorption-free energy, the adsorption equilibrium constant follows:

$$\begin{aligned} \Delta G_{ads}(r) &= -RT \ln K_{ads}(r) = \Delta G_{ads,\infty} - \frac{2\sigma V_M}{r} \\ &= -RT \ln K_{ads,\infty} - \frac{2\sigma V_M}{r} \end{aligned} \tag{2}$$

Thus:

$$K_{ads}(r) = K_{ads,\infty} \exp\left(\frac{2\sigma V_M}{rRT}\right) = K_{ads,\infty} \exp\left(\frac{\eta}{r}\right) \tag{3}$$

where $K_{ads,\infty}$ is size-independent part of thermodynamic adsorption constant, and η is a parameter which is equal to $\eta = 2\sigma V_M/RT$. The size effect on adsorption is derived through the Brønsted–Polanyi relations $k = gK^\chi$ and $k_- = g_-K^{\chi-1}$. Where k is the rate constant, $K = k/k_-$ is thermodynamic equilibrium constant, g and χ are the Brønsted–Polanyi parameters, and $0 < \chi < 1$. This relation used for the explanation of structural activity dependence in homogeneous and heterogeneous catalysis. Thus, the adsorption rate constant for forward and reverse reactions can be reported as [27, 28].

$$\begin{aligned} k(r) &= gK^\chi = gK_{ads,\infty}^\chi \exp\left(\frac{(1-\chi)\eta}{r}\right) \\ &= k_\infty \exp\left(\frac{(1-\chi)\eta}{r}\right) \end{aligned} \tag{4}$$

$$k_-(r) = gK^{\chi-1} = gK_{ads,\infty}^{\chi-1} \exp\left(\frac{-\chi\eta}{r}\right) = k_{-\infty} \exp\left(\frac{-\chi\eta}{r}\right) \tag{5}$$

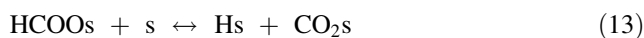
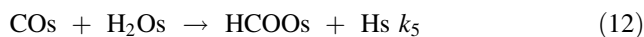
The kinetics of the water–gas shift reaction under Fischer–Tropsch reaction with iron-based catalysts has been studied by many investigators. Development of kinetic model basis of certain mechanism has led to several kinetics models. The formate intermediate and direct oxidation mechanisms for the WGS reaction are proposed in literature [12, 13, 16, 41, 42]. In our previous works, we developed a useful WGS rate expression based on the formate mechanism, which found to provide an improved description of the WGS kinetic data as below [15, 16]:

$$R_{CO_2} = \frac{K_5 K_1 K_3 \left(P_{CO} P_{H_2O} - \frac{P_{CO_2} P_{H_2}}{K_p} \right)}{(1 + K_1 P_{CO} + K_3 P_{H_2O})^2} \tag{6}$$

In these rate equations, P is the partial pressure of species j in the effluent stream and K is the equilibrium constant of the WGS reaction. For the temperature dependency of the equilibrium constant of the WGS reaction, K , the following relation was used [12, 13, 43]:

$$\log K_p = \left(\frac{P_{CO_2} P_{H_2}}{P_{CO} P_{H_2O}} \right)_{eq}, T = \left(\frac{2,073}{T} - 2.029 \right) \tag{7}$$

where K_p is the WGS equilibrium constant at the temperature T . The reaction rate of CO_2 formation is calculated from a material balance over the reactor, assuming ideal gas behavior. This equation obtained from a set of basic reaction as follow. The rate-determining step is assumed to be formate formation step (step 5) in the mechanism.



As discussed in previous paragraph, the Gibbs free energy for steps 1 and 3 can be written as $\Delta G_1 = \Delta G_{1\infty} - \delta(r)$ and $\Delta G_3 = \Delta G_{3\infty} - \delta(r)$. Following the same approach as discussed above for the size-dependent adsorption rates and making use of Eqs. (4) and (5) we can write:

$$K_1(r) = \frac{k_1(r)}{k_{-1}(r)} = \frac{k_1 \exp((1-\chi)\eta/r)}{k_{-1} \exp(-\chi\eta/r)} = K_{1\infty} \exp(\eta/r) \tag{14}$$

$$K_3(r) = \frac{k_3(r)}{k_{-3}(r)} = \frac{k_3 \exp((1-\chi)\eta/r)}{k_{-3} \exp(-\chi\eta/r)} = K_{3\infty} \exp(\eta/r) \tag{15}$$

For evaluation of Gibbs free energy of formate formation (Eq. 12), the overall reaction can be assumed as below:



Thus, the overall Gibbs free energy for formate formation can be evaluated as below:

$$\Delta G_5 = \Delta G_1 + \Delta G_2 \tag{17}$$

$$\Delta G_5 = \Delta G_{5\infty} - 2\delta(r) \tag{18}$$

Thus, for rate constant (k_5) of WGS reaction rates based on previous mechanism can be shown by $k(r)$ and written as below:

$$k(r) = gK^{2(1-\chi)} = k_{\infty} \exp\left(\frac{2(1-\chi)\eta}{r}\right) \quad (19)$$

Using Eqs. (14), (15) and (19), the size-dependent thermodynamics parameters can be evaluated by considering the experimental results. The parameters of model were calculated with the Levenberg–Marquardt (LM) algorithm. The mean absolute relative residual (MARR) is reported as a measure of the goodness of the fit:

$$\text{MARR} = 100 \sum_{i=1}^n \left| \left(\frac{R_{\text{exp}} - R_{\text{mod}}}{R_{\text{exp}}} \right) \right| \frac{1}{n} \quad (20)$$

where n is the number of data points included.

Results and discussion

Water–gas shift activity

During the activation of Fe-based catalyst, hematite (Fe_2O_3) changed to magnetite (Fe_3O_4) and then to iron carbides. Literatures suggested that magnetite (Fe_3O_4) is the most active phase for WGS reaction in Fe-based catalysts [7, 12, 13, 42, 44, 45]. It is well known that during transformation of hematite to magnetite, volumetric changes occurred in catalyst particles. Thus, for size-dependent calculation of WGS kinetic parameters, the size of magnetite (Fe_3O_4) particles must be considered.

The CO_2 formation rates are calculated from a material balance over the reactor by assuming ideal gas behavior and be considered as WGS rates as below:

$$r_{\text{WGS}} = r_{\text{CO}_2} \quad (21)$$

The calculated WGS rates using of Eq. (21) in various temperatures are shown in Fig. 1. In this Fig, the effect of particle sizes on WGS reaction rates is shown and r is the dimension of active phase in WGS reaction (i.e., Fe_3O_4).

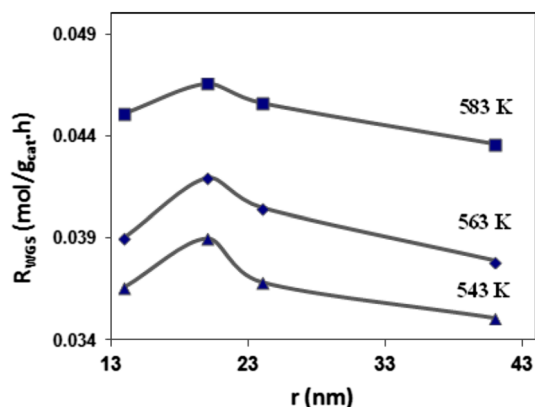


Fig. 1 The effects of temperature and catalyst particle size on WGS reaction rates

As shown in Fig. 1, the WGS reaction rates increased by increasing the temperature and passed from a maximum by decreasing the particle size.

The experimental WGS rates fitted to various kinetic models proposed in literature. In our previous work, we developed a useful kinetic equation for lanthanum-promoted iron catalyst (Eq. 6) [15, 16]. The parameters of the model which are calculated from the experimental data at various temperatures are listed in Table 1 and shown in Figs 2, 3 and 4. These results depicted that by reducing the catalyst particle size, both the rate constant (k) and the adsorption parameters (K_1 and K_3) increased, simultaneously. With respect to model Eqs. (8–13), K_1 is adsorption equilibrium of carbon monoxide and K_3 is adsorption equilibrium of water. These results can explain the complicated manner of WGS rate against the catalyst particle size. Equation (6) predicted that the WGS rate over the iron catalyst increased by increasing of WGS rate constant (k) and decreased by increasing of adsorption parameters (K_1 and K_3) in denominator. But, in Eq. (6) the denominator is to the power of 2, and thus its importance is increasing rapidly. As shown in Fig. 1, by decreasing the catalyst particle size, the WGS reaction rate passed from a maximum. Before the maximum, the WGS reaction increased by increasing the rate constant (k). But after the maximum, the WGS reaction controlled by adsorption parameters (K_1 and K_3). Thus, by increasing the adsorption parameters (K_1 and K_3) of carbon monoxide and water, the reaction rate decreased.

The activation energy of WGS reaction can be determined from calculated rate constant (k), using the Arrhenius equation:

$$k = k_0 \exp\left(\frac{-E_A}{RT}\right) \quad (22)$$

The calculated activation energies for WGS reaction are listed in Table 1. As shown in this table, the activation energies calculated about 83–68 kJ/mol. These activation energies are in excellent agreement with those reported in literatures [12, 13, 42]. As shown in Table 1, the activation energy increased with increase in catalyst particle size (r).

Adsorption enthalpy ΔH_{ads} for carbon monoxide and water can be determined with adsorption parameters (K_1 and K_3) via another Arrhenius type equation:

$$K = K_0 \exp\left(\frac{-\Delta H_{\text{ads}}}{RT}\right) \quad (23)$$

The apparent heats of adsorption for the overall reaction are listed in Table 1. The heats of adsorption for carbon monoxide are calculated about 22–28 kJ/mol and for water are about 94–75 kJ/mol. These results predicted that the heats of adsorptions for water are about 72–46 kJ/mol larger than carbon monoxide (using this model). As shown

Table 1 Calculated WGS kinetic parameters

Catalyst particle size (nm)	k (mol/g _{cat} h bar)			K_1 (bar)			K_3 (bar)			E_a (kJ/mol)	ΔH_1 (kJ/mol)	ΔH_3 (kJ/mol)
	543 K	563 K	583 K	543 K	563 K	583 K	543 K	563 K	583 K			
41	0.357	0.710	1.250	0.427	0.560	0.650	4.414	10.914	18.345	83	28	94
24	0.423	0.816	1.390	0.510	0.680	0.780	5.121	11.786	17.768	78	27	82
20	0.500	0.930	1.500	0.620	0.790	0.910	5.964	13.506	19.947	72	25	80
14	0.580	0.980	1.620	0.720	0.910	1.010	8.579	17.579	26.568	68	22	75

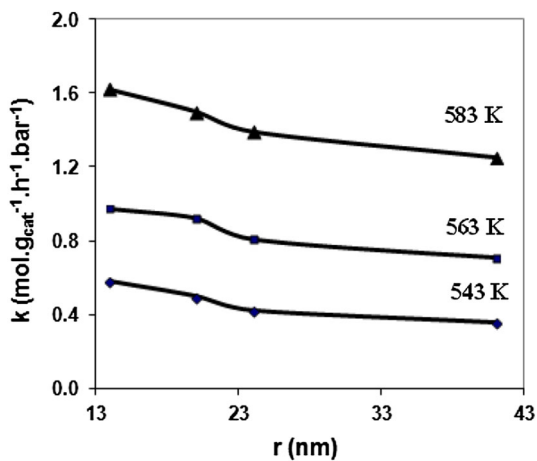


Fig. 2 The calculated WGS rate constant (k) at various temperatures for catalysts

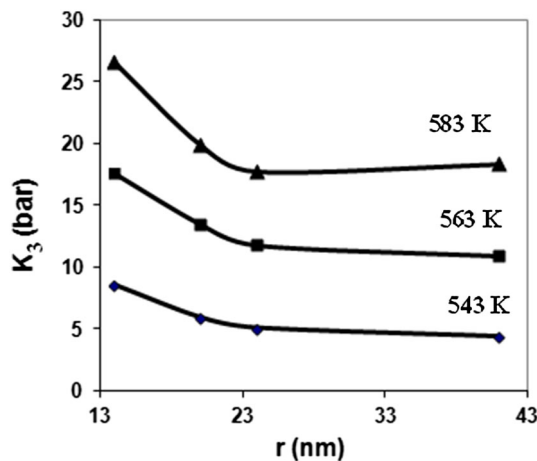


Fig. 4 The calculated adsorption parameter (K_3) at various temperatures for catalysts

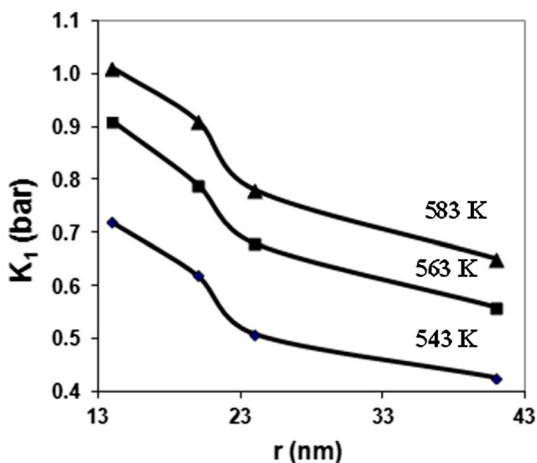


Fig. 3 The calculated adsorption parameter (K_1) at various temperatures for catalysts

in Table 1, the heat of adsorption increased with increase in catalyst particle size (r).

Size-dependent evaluation

Coloration between the rate of heterogeneous reaction and particle size of the active phase of catalyst (e.g., metal) can

be estimated using the standard thermodynamic potential of the catalytically active phase. For evaluation of thermodynamic size-dependent parameters of WGS reaction (like as surface tension σ and η), the size-dependent WGS rate constant given in Eq. (19) is linearized by rearrangement as:

$$\ln k(r) = \ln k_\infty + \frac{2(1 - \chi)\eta}{r} \tag{24}$$

Also the size-dependent of water and carbon monoxide adsorptions constant (K_1 and K_3) are linearized by rearrangement as:

$$\ln K_1(r) = \ln K_{1\infty} + \frac{\eta}{r} \tag{25}$$

$$\ln K_3(r) = \ln K_{3\infty} + \frac{\eta}{r} \tag{26}$$

Hence, a plot of $\ln k(r)$, $\ln K_1(r)$ and $\ln K_3(r)$ versus $1/r$ should give a straight line with intercepts of $\ln k_\infty$, $\ln K_{1\infty}$ and $\ln K_{3\infty}$, and slopes of $2(1 - \chi)\eta$ and η , respectively. Figures 5, 6 and 7 show the plots of the Eqs. (24), (25) and (26) for various iron-based catalysts. The η is a parameter equal to $\eta = 2\sigma V_M/RT$ and by evaluation of η , the surface tension energy (σ) for magnetite phase in lanthanum-promoted iron catalyst can be calculated. The

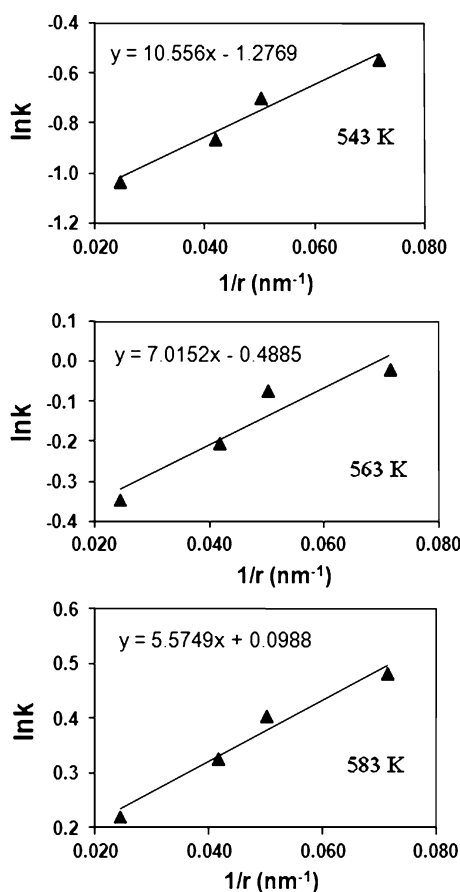


Fig. 5 The linearized plots of the $\ln k(r)$ versus $1/r$ for the various iron-based catalysts

calculated thermodynamic size-dependent parameters are listed in Table 2. This table shows that both size-independent WGS reaction rate constant (k_∞) and size-independent adsorption constants ($K_{1\infty}$ and $K_{3\infty}$) increased with increasing the reaction temperature. Also Table 2 dictated that the η parameter and surface tension energy (σ) for magnetite phases in lanthanum-promoted iron catalyst decreased by increasing the reaction temperature.

In Table 2, the calculated adsorption constants ($K_{1\text{cal}}$ and $K_{3\text{cal}}$) are listed. These parameters calculated using Eqs. (14) and (15) and surface tension energy (σ) for magnetite, which derived from experimental data and Eq. (24). The calculated adsorption constants ($K_{1\text{cal}}$ and $K_{3\text{cal}}$) in Table 2 are good agreement with experimental data in Table 1. These results explained that the calculated surface tension energy (σ) for magnetite phase using Eq. (26) is correct and can be used for calculation of adsorption constants ($K_{1\text{cal}}$ and $K_{3\text{cal}}$).

Table 3 listed the size-independent activation energy (E_∞) and size-independent adsorption enthalpies ($\Delta H_{1\infty}$ and $\Delta H_{3\infty}$). These parameters are calculated from two

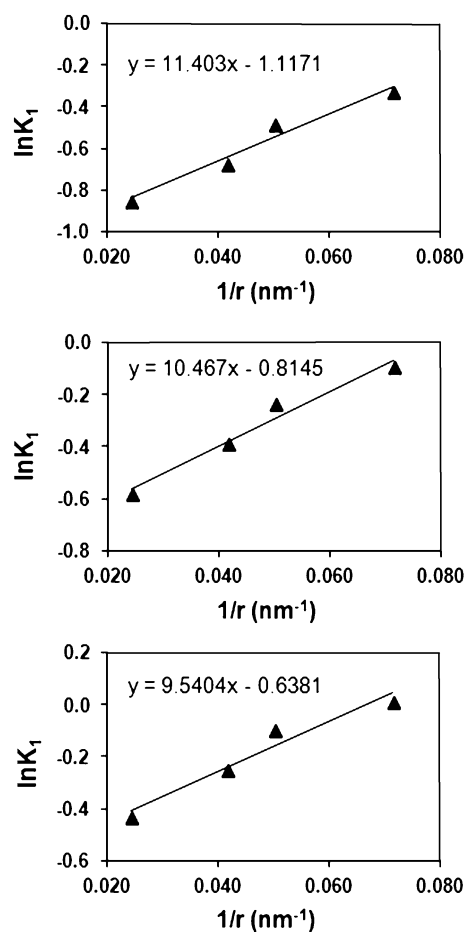


Fig. 6 The linearized plots of the $\ln K_1(r)$ versus $1/r$ for the various iron-based catalysts

ways, first extrapolated the plot of size-dependent activation energies (Fig. 8) and size-dependent adsorption enthalpies (Figs. 9, 10) against $1/r$ to $1/r = 0$ ($r = \infty$). In the second way, the size-independent WGS reaction rate constant (k_∞) and size-independent adsorption constants ($K_{1\infty}$ and $K_{3\infty}$) are calculated from the Arrhenius equation. Figure 11 shows the plot of $\ln(k_\infty)$ versus $1/T$ that gives a straight line with slope of $-E_\infty/R$ and Figs. 12 and 13 show the plot of $\ln(K_{1\infty})$ and $\ln(K_{3\infty})$ versus $1/T$ that give a straight line with slope of $-\Delta H_{1\infty}/R$ and $-\Delta H_{3\infty}/R$, respectively. As listed in Table 3, both the two methods give the same size-independent activation energy (E_∞) and size-independent adsorption enthalpies ($\Delta H_{1\infty}$ and $\Delta H_{3\infty}$), which are equal to 91, 32 and 101 kJ/mol, respectively.

First step in size-dependent evaluation of activation energy and adsorption enthalpy is calculating the temperature-independent surface tension energy (σ_∞). Using calculated temperature-dependent results for η ($\eta = 2\sigma V_M/RT$) listed in Table 3, the temperature-independent surface

tension energy (σ_∞) for iron catalyst can be calculated. Figure 14 shows the variation of η against the temperature and surface tension energy (σ_∞) for iron catalyst that calculated from the slope of plot. The surface tension energy for magnetite phase in lanthanum-promoted iron catalyst calculated equals to 1.37 kJ/cm². Equations (14), (15) and (19) predicted that the size-dependent activation energy and adsorption enthalpy of iron catalysts can be evaluated as below:

$$\Delta H(r) = \Delta H_\infty - \frac{2\sigma V_M}{r} \tag{27}$$

$$E_a(r) = E_{a\infty} - \frac{4(1 - \chi)\sigma V_M}{r} \tag{28}$$

The calculated results for size-dependent activation energy and adsorption enthalpy of iron catalysts are listed in Table 3. By comparison with experimental data in Table 1, it is seen that the calculated activation energy and adsorption enthalpy agree with experimental results.

The results predicted that the surface tension plays an important role in heterogeneous catalytic reaction and many of catalytic phenomenons can be interpreted by this parameter. Surface tension is always positive and depends only on the temperature. The physical dimension of surface tension is energy per unit area (and also force per unit length).

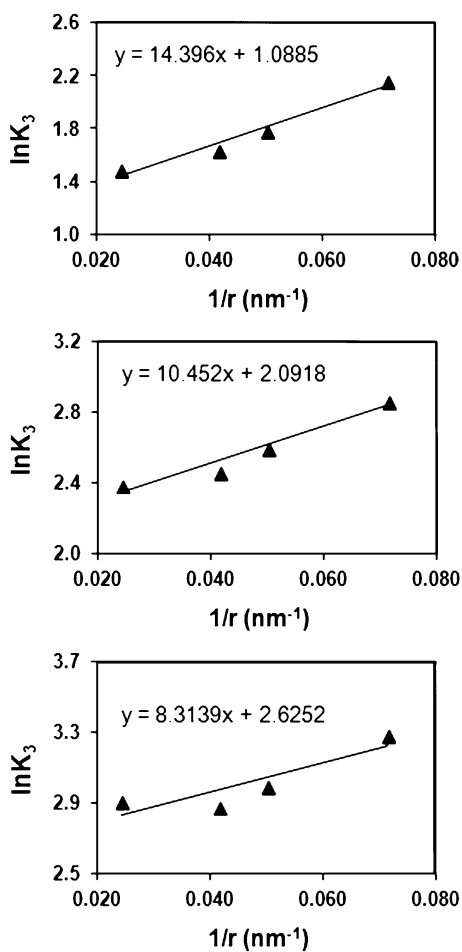


Fig. 7 The linearized plots of the $\ln K_3(r)$ versus $1/r$ for the various iron-based catalysts

Conclusions

Thermodynamic analysis of the particle size effects on kinetics parameters of WGS reaction in FT synthesis is studied on lanthanum-promoted iron catalysts. The

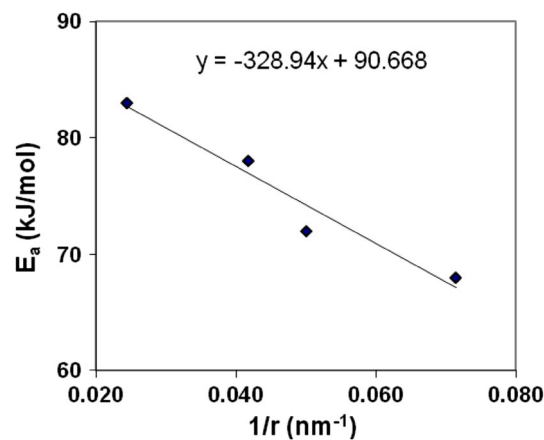


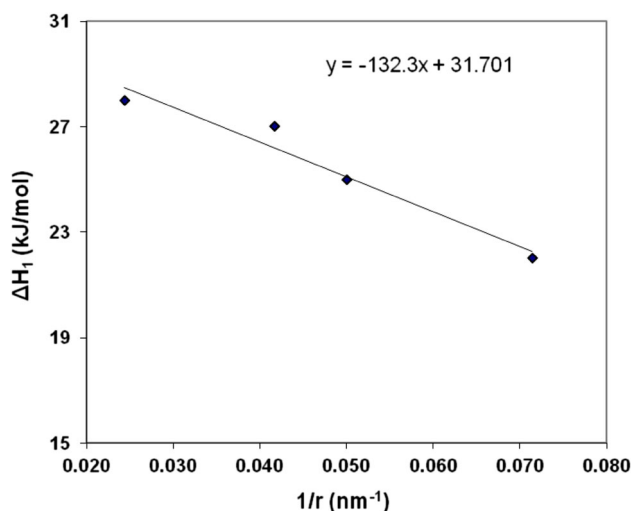
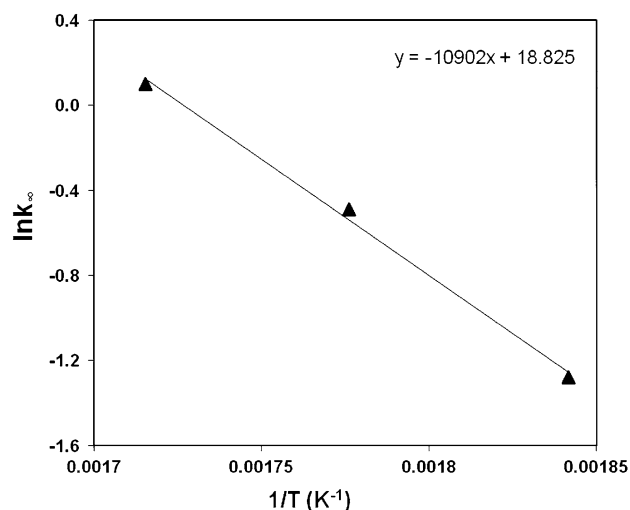
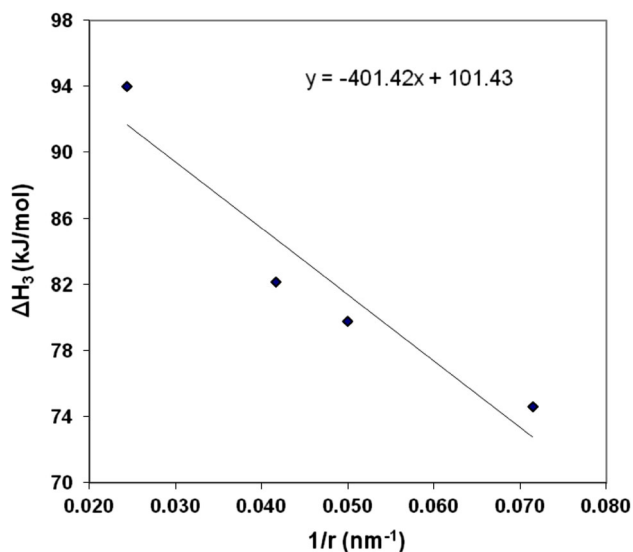
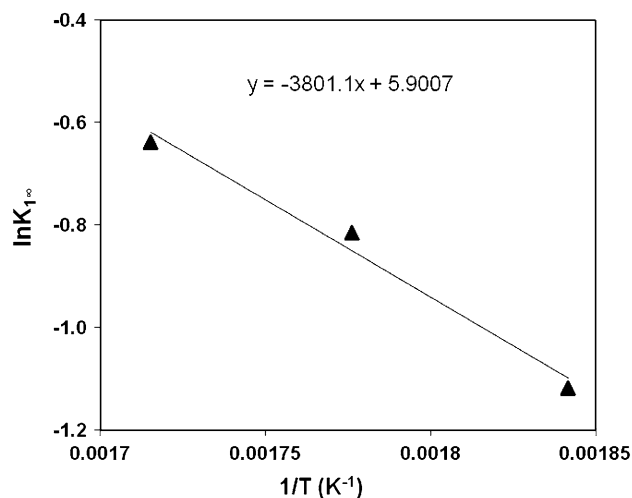
Fig. 8 WGS activation energies for various catalysts as function of catalyst particle size (r)

Table 2 Calculated thermodynamic size-dependent parameters

T	K_{1cal} (bar)				K_{3cal} (bar)				σ (J cm ⁻²)	χ	k_∞ (mol g _{cat} ⁻¹ h ⁻¹ bar ⁻¹)	η (nm)	$K_{1\infty}$ (bar)	$K_{3\infty}$ (bar)
	41 nm	24 nm	20 nm	14 nm	41 nm	24 nm	20 nm	14 nm						
583	0.43	0.53	0.58	0.74	3.92	4.78	5.25	6.71	518	0.54	1.10	9.5	0.53	13.81
563	0.57	0.68	0.75	0.94	10.45	12.53	13.67	17.11	549	0.66	0.61	10.5	0.44	8.10
543	0.67	0.79	0.85	1.04	17.42	20.55	22.25	27.29	577	0.77	0.28	11.4	0.33	2.97

Table 3 Calculated activation energies and enthalpies using size-dependent parameters

E_a Cal (kJ/mol)				ΔH_1 Cal (kJ/mol)				ΔH_3 Cal (kJ/mol)				δ_∞ kJ/ cm ²	$\Delta H_{1\infty}$ (kJ/ mol)	$\Delta H_{3\infty}$ (kJ/ mol)	$E_{a\infty}$ (kJ/ mol)
41 nm	24 nm	20 nm	14 nm	41 nm	24 nm	20 nm	14 nm	41 nm	24 nm	20 nm	14 nm				
85	81	79	73	29	27	26	23	98	96	95	93	1.37	32	101	91

**Fig. 9** Adsorption enthalpy ΔH_1 as function of catalyst particle size (r)**Fig. 11** Size-independent WGS reaction rate constant ($\ln k_\infty$) as function of temperature**Fig. 10** Adsorption enthalpy ΔH_3 as function of catalyst particle size (r)**Fig. 12** Size-independent adsorption parameter ($\ln K_{1\infty}$) as function of temperature

experimental results showed the WGS reaction rates passed from a maximum by decreasing the catalyst particle size. By decreasing the catalyst particle size, not only adsorption

equilibrium but also kinetic rate constant increased. The key in thermodynamic analysis is description of influence of the nanometric size of particles on the chemical

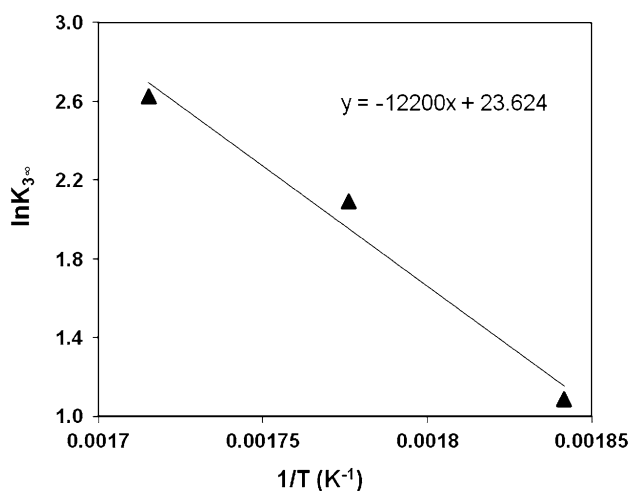


Fig. 13 Size-independent adsorption parameter ($\ln K_{3\infty}$) as function of temperature

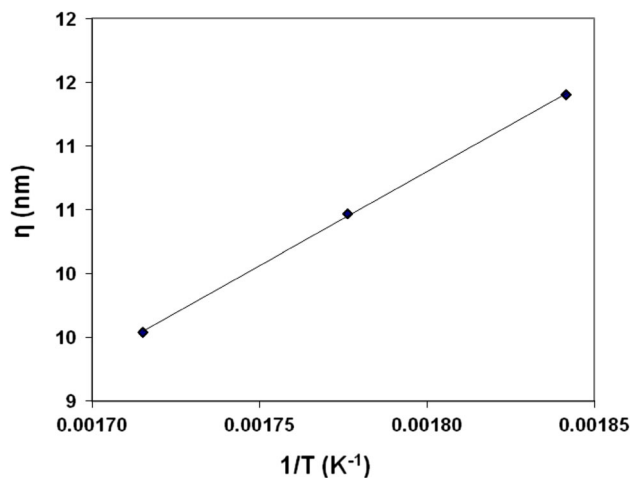


Fig. 14 Calculation of temperature-independent η parameter

potential of the active phase (e.g., clusters supported on a carrier).

References

1. A.K. Dalai, B.H. Davis, Fischer–Tropsch synthesis: a review of water effects on the performances of unsupported and supported Co catalysts. *Appl. Catal. A* **348**(1), 1–15 (2008)
2. B. Davis, Fischer–Tropsch synthesis: overview of reactor development and future potentialities. *Top. Catal.* **32**(3–4), 143–168 (2005)
3. M.E. Dry, The Fischer–Tropsch process: 1950–2000. *Catal. Today* **71**(3–4), 227–241 (2002)
4. M.E. Dry, Practical and theoretical aspects of the catalytic Fischer–Tropsch process. *Appl. Catal. A* **138**(2), 319–344 (1996)

5. M.E. Dry, Present and future applications of the Fischer–Tropsch process. *Appl. Catal. A* **276**(1–2), 1–3 (2004)
6. X. An, B.-S. Wu, H.-J. Wan, T.-Z. Li, Z.-C. Tao, H.-W. Xiang, Y.-W. Li, Comparative study of iron-based Fischer–Tropsch synthesis catalyst promoted with potassium or sodium. *Catal. Commun.* **8**(12), 1957–1962 (2007)
7. M. Dry, Fischer–Tropsch synthesis over iron catalysts. *Catal. Lett.* **7**(1–4), 241–251 (1990)
8. S.A. Eliason, C.H. Bartholomew, Kinetics and deactivation of unpromoted and potassium-promoted iron Fischer–Tropsch catalysts at low pressure (1 Atm), in *Studies in Surface Science and Catalysis*, vol. 68, ed. by H.B. Calvin, B.B. John (Elsevier, New York, 1991), pp. 211–218
9. S. Li, S. Krishnamoorthy, A. Li, G.D. Meitzner, E. Iglesia, Promoted iron-based catalysts for the Fischer–Tropsch synthesis: design, synthesis, site densities, and catalytic properties. *J. Catal.* **206**(2), 202–217 (2002)
10. A. Nakhaei Pour, S.M.K. Shahri, H.R. Bozorgzadeh, Y. Zamani, A. Tavasoli, M.A. Marvast, Effect of Mg, La and Ca promoters on the structure and catalytic behavior of iron-based catalysts in Fischer–Tropsch synthesis. *Appl. Catal. A Gen.* **348**(2), 201–208 (2008)
11. A. Sarkar, D. Seth, A. Dozier, J. Neathery, H. Hamdeh, B. Davis, Fischer–Tropsch synthesis: morphology, phase transformation and particle size growth of nano-scale particles. *Catal. Lett.* **117**(1–2), 1–17 (2007)
12. G.P. Van Der Laan, A.A.C.M. Beenackers, Kinetics and selectivity of the Fischer–Tropsch synthesis: a literature review. *Catal. Rev.* **41**(3–4), 255–318 (1999)
13. G.P. van der Laan, A.A.C.M. Beenackers, Intrinsic kinetics of the gas–solid Fischer–Tropsch and water gas shift reactions over a precipitated iron catalyst. *Appl. Catal. A* **193**(1–2), 39–53 (2000)
14. A.N. Pour, M.R. Housaindokht, J. Zarkesh, M. Irani, E.G. Babakhani, Kinetics study of CO hydrogenation on a precipitated iron catalyst. *J. Ind. Eng. Chem.* **18**(2), 597–603 (2012)
15. A. Nakhaei Pour, M.R. Housaindokht, J. Zarkesh, S.F. Tayyari, Water–gas–shift kinetic over nano-structured iron catalyst in Fischer–Tropsch synthesis. *J. Nat. Gas Sci Eng* **2**(2–3), 79–85 (2010)
16. A. Nakhaei Pour, M.R. Housaindokht, S.F. Tayyari, J. Zarkesh, S.M.K. Shahri, Water–gas–shift kinetics over a Fe/Cu/La/Si catalyst in Fischer–Tropsch synthesis. *Chem. Eng. Res. Des.* **89**(3), 262–269 (2011)
17. A.T. Bell, The impact of nanoscience on heterogeneous catalysis. *Science* **299**(5613), 1688–1691 (2003)
18. T. Bernhardt, U. Heiz, U. Landman, Chemical and catalytic properties of size-selected free and supported clusters, in *Nanocatalysis*, ed. by U. Heiz, U. Landman (Springer, Berlin, Heidelberg, 2007), pp. 1–191
19. C.Q. Sun, Size dependence of nanostructures: impact of bond order deficiency. *Prog. Solid State Chem.* **35**(1), 1–159 (2007)
20. X. Zhou, W. Xu, G. Liu, D. Panda, P. Chen, Size-dependent catalytic activity and dynamics of gold nanoparticles at the single-molecule level. *J. Am. Chem. Soc.* **132**(1), 138–146 (2009)
21. A.N. Pour, M.R. Housaindokht, S.M.K. Shahri, E.G. Babakhani, M. Irani, Size dependence on reduction kinetic of iron based Fischer–Tropsch catalyst. *J. Ind. Eng. Chem.* **17**(3), 596–602 (2011)
22. A.N. Pour, M.R. Housaindokht, S.F. Tayyari, J. Zarkesh, Effect of nano-particle size on product distribution and kinetic parameters of Fe/Cu/La catalyst in Fischer–Tropsch synthesis. *J. Nat. Gas Chem.* **19**(2), 107–116 (2010)
23. A. Nakhaei Pour, M.R. Housaindokht, The olefin to paraffin ratio as a function of catalyst particle size in Fischer–Tropsch synthesis by iron catalyst. *J. Nat. Gas Sci. Eng.* **14**, 204–210 (2013)
24. A. Nakhaei Pour, M. Housaindokht, Fischer–Tropsch synthesis over CNT supported cobalt catalysts: role of metal nanoparticle

- size on catalyst activity and products selectivity. *Catal. Lett.* **143**, 1328–1338 (2013)
25. V.N. Parmon, Thermodynamic analysis of the effect of the nanoparticle size of the active component on the adsorption equilibrium and the rate of heterogeneous catalytic processes. *Dokl. Phys. Chem.* **413**(1), 42–48 (2007)
 26. D. Murzin, Size dependent interface energy and catalytic kinetics on non-ideal surfaces. *React. Kinet. Catal. Lett.* **97**(2), 165–171 (2009)
 27. D.Y. Murzin, Thermodynamic analysis of nanoparticle size effect on catalytic kinetics. *Chem. Eng. Sci.* **64**(5), 1046–1052 (2009)
 28. D.Y. Murzin, Kinetic analysis of cluster size dependent activity and selectivity. *J. Catal.* **276**(1), 85–91 (2010)
 29. D.Y. Murzin, I.L. Simakova, On quantitative description of metal particles size effect in catalytic kinetics. *Kinet. Catal.* **51**(6), 828–831 (2010)
 30. A. Nakhaei Pour, M. Housaindokht, A. Behroozsarand, M. Khodagholi, Thermodynamic analysis of nanoparticle size effect on kinetics in Fischer–Tropsch synthesis by lanthanum promoted iron catalyst. *Appl. Phys. A* (2013). doi:10.1007/s00339-013-8156-7
 31. A. Nakhaei Pour, M.R. Housaindokht, M. Irani, S.M. Kamali Shahri, Size-dependent studies of Fischer–Tropsch synthesis on iron based catalyst: new kinetic model. *Fuel* **116**, 787–793 (2014)
 32. A.N. Pour, S. Taghipoor, M. Shekariz, S.M.K. Shahri, Y. Zamani, Fischer–Tropsch synthesis with Fe/Cu/La/SiO₂ nano-structured catalyst. *J. Nanosci. Nanotechnol.* **9**(7), 4425–4429 (2009)
 33. T. Herranz, S. Rojas, F.J. Pérez-Alonso, M. Ojeda, P. Terreros, J.L.G. Fierro, Hydrogenation of carbon oxides over promoted Fe–Mn catalysts prepared by the microemulsion methodology. *Appl. Catal. A* **311**, 66–75 (2006)
 34. A.N. Pour, M.R. Housaindokht, S.F. Tayyari, J. Zarkesh, Fischer–Tropsch synthesis by nano-structured iron catalyst. *J. Nat. Gas Chem.* **19**(3), 284–292 (2010)
 35. A.N. Pour, M.R. Housaindokht, S.F. Tayyari, J. Zarkesh, Deactivation studies of nano-structured iron catalyst in Fischer–Tropsch synthesis. *J. Nat. Gas Chem.* **19**(3), 333–340 (2010)
 36. M. Ding, Y. Yang, B. Wu, T. Wang, L. Ma, H. Xiang, Y. Li, Transformation of carbonaceous species and its influence on catalytic performance for iron-based Fischer–Tropsch synthesis catalyst. *J. Mol. Catal. A: Chem.* **351**, 165–173 (2011)
 37. M. Ding, Y. Yang, B. Wu, T. Wang, H. Xiang, Y. Li, Effect of reducing agents on microstructure and catalytic performance of precipitated iron–manganese catalyst for Fischer–Tropsch synthesis. *Fuel Process. Technol.* **92**(12), 2353–2359 (2011)
 38. M.R. Housaindokht, Nakhaei Pour, A., Study the effect of HLB of surfactant on particle size distribution of hematite nanoparticles prepared via the reverse microemulsion. *Solid State Sci.* **14**(5), 622–625 (2012)
 39. M.R. Housaindokht, A.N. Pour, Precipitation of hematite nanoparticles via reverse microemulsion process. *J. Nat. Gas Chem.* **20**(6), 687–692 (2011)
 40. A. Nakhaei Pour, M.R. Housaindokht, S.F. Tayyari, J. Zarkesh, M.R. Alaei, Deactivation studies of Fischer–Tropsch synthesis on nano-structured iron catalyst. *J. Mol. Catal. A Chem.* **330**(1–2), 112–120 (2010)
 41. A.N. Pour, M.R. Housaindokht, S.F. Tayyari, J. Zarkesh, Kinetics of the water–gas shift reaction in Fischer–Tropsch synthesis over a nano-structured iron catalyst. *J. Nat. Gas Chem.* **19**(4), 362–368 (2010)
 42. B.-T. Teng, J. Chang, C.-H. Zhang, D.-B. Cao, J. Yang, Y. Liu, X.-H. Guo, H.-W. Xiang, Y.-W. Li, A comprehensive kinetics model of Fischer–Tropsch synthesis over an industrial Fe–Mn catalyst. *Appl. Catal. A* **301**(1), 39–50 (2006)
 43. Y.-N. Wang, W.-P. Ma, Y.-J. Lu, J. Yang, Y.-Y. Xu, H.-W. Xiang, Y.-W. Li, Y.-L. Zhao, B.-J. Zhang, Kinetics modelling of Fischer–Tropsch synthesis over an industrial Fe–Cu–K catalyst. *Fuel* **82**(2), 195–213 (2003)
 44. S. Krishnamoorthy, A. Li, E. Iglesia, Pathways for CO₂ formation and conversion during Fischer–Tropsch synthesis on iron-based catalysts. *Catal. Lett.* **80**(1–2), 77–86 (2002)
 45. N. Sirimanothan, H. Hamdeh, Y. Zhang, B. Davis, Fischer–Tropsch synthesis: changes in phase and activity during use. *Catal. Lett.* **82**(3–4), 181–191 (2002)